Statistical assessment of turbulence homogeneity for the head of gravity currents

J. Pelmard[1], S.E. Norris[2] and H. Friedrich[1]

[1]Department of Civil and Environment Engineering
University of Auckland, Auckland 1142, New Zealand

[2]Department of Mechanical Engineering
University of Auckland, Auckland 1142, New Zealand

Abstract

We show that meaningful turbulence statistics can be obtained for gravity currents, in particular turbidity currents, by applying streamwise and spanwise spatial averaging over a carefully-chosen region of the current's head. The current structure is generally depicted as having a compact head, followed by a decaying body and an almost non-turbulent tail. Due to the transient nature of turbidity currents, it is difficult to quantify the turbulence of the inner current, since the inability to calculate temporally averaged statistics prevents the quantification of the mass and momentum flux exchanges in this region. For a $Re_b = 60,000$ lock-exchange current, we demonstrate that spatial averaged statistics from a single run are consistent with those from an ensemble average of 200 runs. Slight discrepancies are observed, showing the limits of the hypothesis of spatial homogeneity considered.

Introduction

Gravity currents, also known as density-driven flows, are a type of flow driven by a density gradient due to the infiltration of a dense fluid into a lower density fluid. They are observed in a large range of natural physical conditions. They can be induced by temperature gradients, as observed in atmospheric flows, or caused by in-homogeneities in particle concentrations such as pyroclastic flows. Our specific interest is underwater turbidity currents, in which the particles tend to naturally settle in addition to the buoyant motion [1].

To date, the behaviour of gravity currents has been thoroughly investigated and their general features have been largely addressed experimentally and numerically for the so-called lock-exchange configuration (Figure 1). It consists in suddenly releasing a finite or infinite quantity of dense fluid trapped inside a tank into a channel filled with a lower density fluid, initially separated from the tank by a gate. Comparison of simulation results to empirical datasets has demonstrated the ability of Direct Numerical Simulation (DNS) [2-4], Large Eddy Simulation (LES) [5-8], and more recently Lattice Boltzmann Models (LBM) [9] to accurately predict the turbulent features generating the mixing dynamics of currents, from low Reynolds number laminar flows up to highly turbulent laboratory and river scale currents.
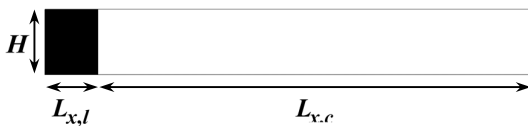
Figure 1. Lock-exchange flume, left (black) the header box, right (white) the flume channel.

Upon the current's release, the dense fluid starts flowing below the ambient fluid, taking the form of a dense head. As the current propagates, large Kelvin-Helmholtz billows start detaching from the head, causing the entrainment of ambient fluid into the current and leaving a large decaying body in the head's wake [8]. The sustainability of the current is intrinsically subjected to its ability to hold a coherent dense head over time, and the mixing in the shear layer at the threshold between the two fluids plays a key role on the current's dilution. Several studies have focused on the qualitative description of the mixing dynamics of gravity currents, based on a description of their vortical turbulent structures [3, 10]. Some attempts have been made to quantify the mixing rate. The global current's dilution is described by the evolution of the entrainment parameter E, characterising the expansion of the current's volume due to the mixing with the ambient fluid [8, 11]. Another measure of mixing is obtained numerically by following the dynamic variation of the background potential energy Ep_r [7], as introduced in the evolution equation derived by Winters et al. [12]. The reference potential energy corresponds to the potential energy attained by a fluid at a specific state moved adiabatically to an equilibrium state. In other words, Ep_r is the minimum potential energy level attained after the conversion of potential energy into kinetic energy, and its increase corresponds to the irreversible production of potential energy due to diffusive mixing.

Those quantities only provide information at the global scale of the current and the local quantification of the flux exchanges are seldom investigated. Indeed, the computation of the turbulence statistics is usually prevented by the transient nature of the flow. A first alternative can be found in averaging over a large ensemble of simulations, however the prohibitively large CPU and storage requirements limits the extension of this method to a systematic approach. In the particular case of a horizontal statistically spatial homogeneous body found in infinitely loaded currents, Cantero et al. [13] overcome the averaging limitations by calculating the turbulent statistics using horizontal spatial averaging and the computation costs were reduced by computing on a significantly reduced domain, which only represented a streamwise section of the current's body. This method has been applied to the study of flux exchanges in the body of particle-driven gravity currents [13-15] and the study of mixing at the interface of settled particles entrained by a turbulent channel flow [16].

In order to analyse the local flux exchanges inside a statistically evolving current, this study aims to discuss the general distribution of the turbulence statistics inside a gravity current in order to present reliable methodologies for their computation on instantaneous fields. To do so, averaging is performed over an ensemble of 200 LES simulations of a fully turbulent lock-exchange problem. From an analysis of the turbulence statistics in the current's head, a region of pseudo-horizontal homogeneity is identified, the statistics for which are compared with those obtained by spatial averaging a single instantaneous field. Using these statistics we introduce a scaling of the mixing layer, potentially allowing the analysis of the statistics in a larger section of the current.

Problem definition and numerical model

The 3D model is based on the standard lock-exchange experiment of Wilson et al. [17]. Relative to the channel's height H, the lock and channel's lengths are taken as $L_{x,l} = 1.933H$ and $L_{x,c} = 16.667H$ and have a width $L_z = 1.333H$. The channel has a downward 2% slope. The header box is filled with sediment-laden fluid of density ρ_1 and the flume channel is filled with the same fluid without sediment of density ρ_0. At $t = 0$, the sediment-laden fluid is released and the current starts flowing into the channel. The problem is described by the continuity and the momentum equations together with a transport equation for the sediment mass fraction m. The coupling is assured by applying the Boussinesq approximation. The equations are presented under their dimensionless form. The scaling quantities are chosen to be half of the channel height $H/2$, the maximum sediment mass fraction m_{max}, the buoyant velocity $u_b = \sqrt{(H/2)\,g'}$ with the reduced gravity $g' = g\,(\rho_1 - \rho_0)$ and the time scale $t_0 = (H/2)/u_b$. The physical conditions are described by the Reynolds number $Re_b = (u_b\,H/2)/\nu$ and Schmidt number $Sc = \nu/\kappa$. Introducing $\overline{}$ as the filter operator, the LES equations are written as

$$\frac{\partial \overline{u_i}}{\partial x_i} = 0 \tag{1}$$

$$\frac{\partial \overline{u_i}}{\partial t} + \frac{\partial (\overline{u_i u_j})}{\partial x_j} = -\frac{\partial \overline{p}}{\partial x_i} + \frac{\partial}{\partial x_j}\left[\frac{1}{Re_b}\frac{\partial \overline{u_i}}{\partial x_j}\right] - \frac{\partial \tau_{ij}}{\partial x_j} + \overline{m} \tag{2}$$

$$\frac{\partial \overline{m}}{\partial t} + \frac{\partial \overline{u_i m}}{\partial x_i} = \frac{\partial}{\partial x_i}\left[\frac{1}{Sc\,Re_b}\frac{\partial \overline{m}}{\partial x_i}\right] - \frac{\partial \tau_i^m}{\partial x_i} \tag{3}$$

The influence of the eliminated turbulent structures on the resolved components remains in the equations through the momentum and concentration residual-stress tensors τ_{ij} and τ_i^m. The closure is made using an eddy viscosity approach using

$$\tau_{ij} = -\nu_t\left(\frac{\partial \overline{u_i}}{\partial x_j} + \frac{\partial \overline{u_j}}{\partial x_i}\right) \text{ and } \tau_i^m = -\kappa_t\frac{\partial \overline{m}}{\partial x_i} \tag{4}$$

The subgrid scale viscosity ν_t is modelled using a standard Smagorinsky model and a turbulent Schmidt number $Sc_t = \nu_t/\kappa_t = 0.7$ is imposed for the calculation of the subgrid scale diffusivity κ_t.

The simulations are performed using the structured non-staggered Cartesian finite volume SnS code developed by Norris [18]. The time step varies to maintain the value of the Courant number (CFL $= u_i\,\Delta t/\Delta x$) within the range $0.15 - 0.25$. The simulations were performed on a $1140 \times (55 + 37) \times 74$ mesh. A uniform grid spacing $\Delta = 0.035$ was chosen in each direction except near the bottom wall. The first grid size at the bottom wall was set to $\Delta y = 0.00133$ to ensure its location in the near-wall viscous sublayer ($y^+ < 5$). The vertical mesh spacing has been progressively increased until reaching $\Delta y = h$ over the layer $0 < y < 0.667$ on 55 cells so the ratio between two consecutive vertical mesh size remains in the range $[0.85; 1.15]$ and the cell size is kept uniform on the 37 remaining cells. Slip wall conditions were imposed at the boundaries except for the bottom boundary which was modelled as a non-slip wall.

Here, a fully turbulent current of $Re_b = 60{,}000$ is considered and the Schmidt number is set to $Sc = 1$ [19]. A set of 200 simulations were initialised with a different random velocity inside the header box for each run. The results have been extracted during the slumping phase of the current's propagation at $t = 29.1$. The statistics are calculated using a combination of averaging over the 200 resulting fields and over the spanwise z-direction of the current. The averaging operator is represented by $\langle\ \rangle$ whereas a "prime" denotes the remaining perturbation. The instantaneous data presented are systematically averaged over the z-direction.

Results and discussion

Turbulence identification

The turbulence of gravity currents is mainly confined in the layer at the interface with the ambient fluid, also called the mixing layer, and is the location of strong vortical motions (fFigure 2a-b). The large Kelvin-Helmholtz billows, as well as the smaller turbulent structures observed on the instantaneous field, are smoothed by the ensemble averaging and are replaced by a smooth layer of vorticity. Defining the mixing layer as the region within which the spanwise vorticity component $\langle \Omega_z \rangle > 0$, it is seen to expand inside the current until reaching the bottom wall and remains quasi-constant after that point. The vorticity is seen to be the strongest at the current's nose and decays whilst moving towards the body. In contrast, the turbulent kinetic energy k peaks inside the head (Figure 2c) at $x = 16.41$. Despite a slight vertical expansion resulting from the mixing layer's enlargement, k exhibits a horizontally pseudo-homogeneous and symmetric streamwise layer around this position. Similar features are observed for the shear-stresses (not shown).
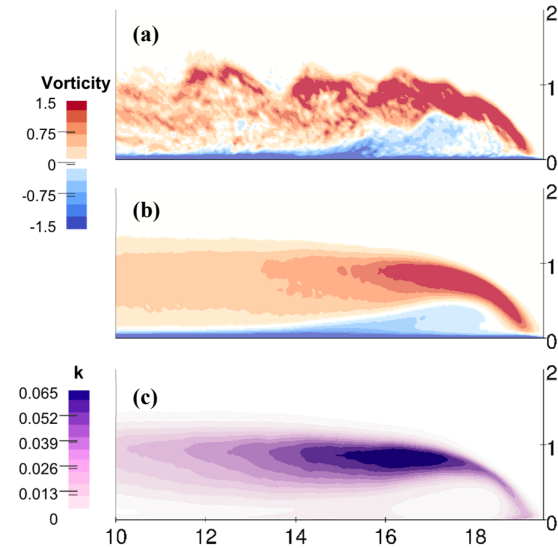
Figure 2. 2D fields of instantaneous vorticity (a), averaged vorticity (b) and turbulence kinetic energy (c).

Turbulence statistics inside the head

The identification of the head/body limit of gravity currents is not trivial. We will define measures based on the current's height h_c, defined as the mean height of the current.

$$h_c(x,t) = \frac{1}{L_y}\int_0^{L_y} \overline{m}\,.dy \tag{5}$$

Experimentalists and numerical modellers commonly define the head-body threshold as the first local minimum of the current's height from the current's leading edge [20, 21]. Figure 3 presents the streamwise profiles of the current's height, superimposed with its equivalent for five instantaneous fields. The limit of the instantaneous fields' head matches with a range of maximum constant $\partial\langle h_c \rangle/\partial x$, equivalent to approximately $H/4$ in the range $15.85 < x < 16.35$. The maximum of turbulence kinetic energy is found inside the head, near the threshold with the body. The pseudo-homogeneous region lasts approximately until $x_{hcm} = 17.3$, corresponding to the maximum of $\langle h_c \rangle$.

In order to qualify the possible computation of the turbulence statistics from spatial averaging, the vertical profiles of the first order statistic $\langle u \rangle$ — the averaged streamwise velocity — and the second order statistics $\langle u'u' \rangle$ and $\langle u'v' \rangle$ — the streamwise velocity perturbation and Reynolds-stress — are presented in Figure 4. The profiles are plotted from the ensemble averaged flow at $x_A = 16.41$, referred as A_{xa}, along with the profiles averaged over three boxes of length $dx = [1; 1.5; 2]$ and centred on x_A for the ensemble averaged field, labelled $[A_1; A_{1.5}; A_2]$, and an instantaneous field, referred as $[I_1; I_{1.5}; I_2]$.
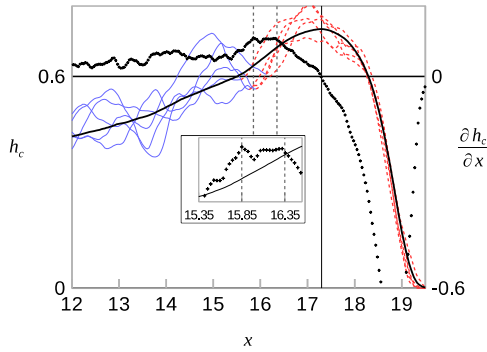
Figure 3. Streamwise profile of $\langle h_c \rangle$ (thick line) and its derivative $\partial \langle h_c \rangle / \partial x$ (+ symbol). Also plotted are five instantaneous profiles of h_c (fine lines). The body is plotted in plain blue, and the head in red dashed lines.

The statistics exhibit the general features found in regular mixing layers [22]. A sharp quasi constant gradient of mean velocity connects the constant velocity of the ambient fluid above the current and the maximum inside the current. The near-wall flow is correctly depicted showing the expected logarithmic expansion after the near-wall viscous region (not shown here). Likewise, the statistics show a large peak inside the mixing layer, before drastically dropping to 0 above the current and at a largely shorter level inside the propagating current.

Regardless of the length of the averaging area, the profiles obtained from the ensemble averaged fields agree well with the profiles A_{xa}, which confirms the pseudo-homogeneous hypothesis. Slight differences are nonetheless observed for $\langle u'v' \rangle$, where averaging leads to an under-prediction of the peak's magnitude. Overall, the profiles obtained from the instantaneous field also show good agreement with the profiles for case A_{xa}. The mean velocity $\langle u \rangle$ is slightly over-predicted at the mixing layer's thresholds, as well as its gradient inside the mixing layer. The profile of $\langle u'u' \rangle$ is reduced at its peak, however the values remain qualitatively in the same range of magnitude as the other profiles and $\langle u'v' \rangle$ suffer of similar under-predictions as profiles A_1, $A_{1.5}$ and A_2. Still, case I_1 fails to correctly predict the positions of the peaks of $\langle u'u' \rangle$ and $\langle u'v' \rangle$, and shows the largest over-estimation of the extrema of $\langle u \rangle$, which may be due to an insufficient number of points to accurately perform the averaging, or the non-symmetry of the data in this region. On the contrary, cases $I_{1.5}$ and I_2 show similar performances, despite $I_{1.5}$ being slightly better on the base of a better estimation of $\langle u'v' \rangle$ peak's magnitude. Consequently, a streamwise averaging box of $dx = H/2$ leads to qualitatively accurate statistics.

Scaling of the mixing layer

Another aspect of the investigation consists of normalising the mixing layer by applying a scaling based on the mixing layer's length. As introduced previously, the mixing layer's length is

here chosen as the region corresponding to $\langle \Omega_z \rangle > 0$. The inner boundary is obtained for $\langle \Omega_z \rangle = 0$. As the vorticity stays positive, but converges to 0 above the current, $\Delta \langle \Omega_z \rangle < 0.01$ is chosen as criterion for the definition of the outer limit of the mixing layer, where $\Delta \langle \Omega_z \rangle$ is the vorticity difference between two consecutive vertical points. This definition is shown to be more relevant than the commonly used definition based on the integral scale of the mean streamwise velocity as it embraces a larger area of the swirling motion.
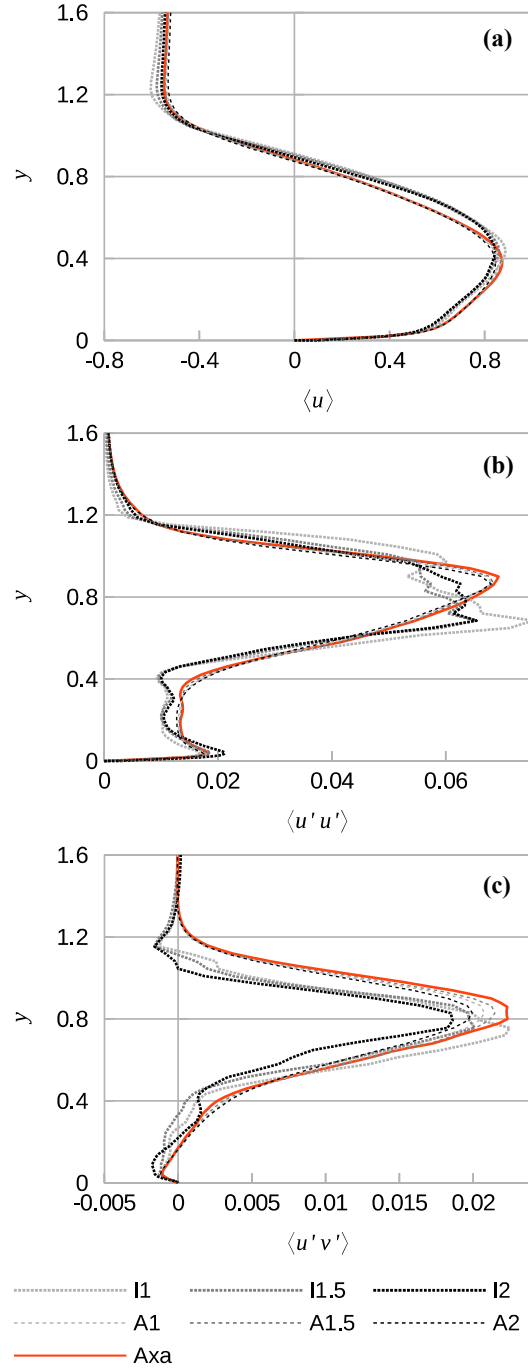
Figure 4. Vertical profiles of mean velocity $\langle u \rangle$ (a), velocity perturbation $\langle u'u' \rangle$ (b) and Reynolds stress $\langle u'v' \rangle$ (c) inside the current's head.

Figure 5 presents the evolution of the streamwise velocity perturbation inside the normalised mixing layer. Although the turbulence decays inside the current's body, horizontal homogeneity of the velocity perturbation scaled by its vertical maximum along the current $\langle u'u'\rangle /\max_y\langle u'u'\rangle$ is observed for $x < x_{hc}$, whereas the scaling quantity $\max_y\langle u'u'\rangle$ decreases linearly as $0.006x$ inside the body. From these observations, further work is needed to assess the possibility of computing the vertical profile of $\langle u'u'\rangle$ by scaling the instantaneous field using the linear $0.006x$ law and rescaling the values to obtain the magnitude at the position desired. The identification of the dependency of the linear law's coefficient on the fluids' features remains as a topic for future investigation.
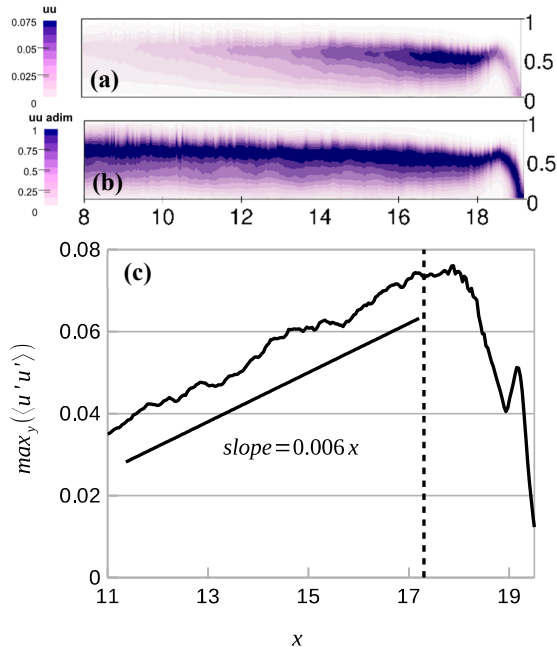
Figure 5. Streamwise velocity perturbation field $\langle u'u'\rangle$ and scaled $\langle u'u'\rangle /\max_y\langle u'u'\rangle$ in the plane $(x; y /lm)$ inside the mixing layer.

Conclusions

A lock-exchange problem, in which a gravity current is generated by a sudden release of a high density fluid into a channel filled with a lower density fluid, has been simulated using a 3D LES model with the finite volume code SnS. Very fine particles are modelled as a Boussinesq gravity current, in which the motion is driven by the density gradients inside the fluid. The homogeneity of the turbulence inside the head is first studied by computing the vertical profiles of the turbulence statistics from an ensemble average of 200 simulations initialised using different random initial velocity distributions. The statistics obtained from spatial averaging inside the head of a single simulation are consistent with their equivalent statistics obtained from the ensemble averaged field.

References

[1] Simpson JE. Gravity Currents in the Laboratory, Atmosphere, and Ocean. *Annu Rev Fluid Mech*. 1982;14:213-34.
[2] Härtel C, Meiburg E, Necker F. Analysis and direct numerical simulation of the flow at a gravity-current head. Part 1. Flow topology and front speed for slip and no-slip boundaries. *J Fluid Mech*. 2000;418:189-212.

[3] Nasr-Azadani M, Meiburg E. Turbidity currents interacting with three-dimensional seafloor topography. *J Fluid Mech*. 2014;745:409-43.
[4] Cantero MI, Balachandar S, Garcia MH. High-resolution simulations of cylindrical density currents. *J Fluid Mech*. 2007;590:437-69.
[5] Ooi SK, Constantinescu G, Weber L. Numerical simulations of lock-exchange compositional gravity current. *J Fluid Mech*. 2009;635:361-88.
[6] Tokyay T, Constantinescu G, Meiburg E. Lock-exchange gravity currents with a low volume of release propagating over an array of obstacles. *J Geophys Res Oceans*. 2014;119:2752-68.
[7] Özgökmen TM, Iliescu T, Fischer PF. Reynolds number dependence of mixing in a lock-exchange system from direct numerical and large eddy simulations. *Ocean Modelling*. 2009;30:190-206.
[8] Ottolenghi L, Adduce C, Inghilesi R, Armenio V, Roman F. Entrainment and mixing in unsteady gravity currents. *J Hydraul Res*. 2016;54:541-57.
[9] Ottolenghi L, Prestininzi P, Montessori A, Adduce C, La Rocca M. Lattice Boltzmann simulations of gravity currents. *European Journal of Mechanics-B/Fluids*. 2018;67:125-36.
[10] Cantero MI, Balachandar S, Garcia MH, Bock D. Turbulent structures in planar gravity currents and their influence on the flow dynamics. *J Geophys Res Oceans*. 2008;113.
[11] Krug D, Holzner M, Luthi B, Wolf M, Kinzelbach W, Tsinober A. Experimental study of entrainment and interface dynamics in a gravity current. *Experiments in Fluids*. 2013;54:1530.
[12] Winters KB, Lombard PN, Riley JJ, Dasaro EA. Available Potential-Energy and Mixing in Density-Stratified Fluids. *J Fluid Mech*. 1995;289:115-28.
[13] Cantero MI, Balachandar S, Parker G. Direct numerical simulation of stratification effects in a sediment-laden turbulent channel flow. *J Turbul*. 2009;10:1-28.
[14] Cantero MI, Shringarpure M, Balachandar S. Towards a universal criteria for turbulence suppression in dilute turbidity currents with non-cohesive sediments. *Geophys Res Lett*. 2012;39.
[15] Shringarpure M, Cantero MI, Balachandar S. Equivalence of turbulence statistics between monodisperse and polydisperse turbidity currents. *Advances in Water Resources*. 2017.
[16] Salinas JS, Shringarpure M, Cantero MI, Balachandar S. Mixing at a sediment concentration interface in turbulent open channel flow. *Environ Fluid Mech*. 2018;18:173-200.
[17] Wilson RI, Friedrich H, Stevens C. Turbulent entrainment in sediment-laden flows interacting with an obstacle. *Phys Fluids*. 2017;29:036603.
[18] Norris S. A Parallel Navier–Stokes Solver for Natural Convection and Free Surface Flow [PhD Thesis]: University of Sydney; 2000.
[19] Bonometti T, Balachandar S. Effect of Schmidt number on the structure and propagation of density currents. *Theor Comput Fluid Dyn*. 2008;22:341-61.
[20] Hartel C, Carlsson F, Thunblom M. Analysis and direct numerical simulation of the flow at a gravity-current head. Part 2. The lobe-and-cleft instability. *J Fluid Mech*. 2000;418:213-29.
[21] Nogueira HIS, Adduce C, Alves E, Franca MJ. Dynamics of the head of gravity currents. *Environ Fluid Mech*. 2014;14:519-40.
[22] Yang W, Zhang H, Chan C, Lin W. Large eddy simulation of mixing layer. *Journal of computational and applied mathematics*. 2004;163:311-8.